1-1-1997

Irreversible critical current and the anomalous magnetic-moment peak in silver-sheathed (Pb,Bi)2Sr2Ca2Cu3O10 + y tapes

K. H. Muller
CSIRO, Australia

C. Andrikidis
CSIRO, Australia

Y. C. Guo
University of Wollongong

Irreversible critical current and the anomalous magnetic-moment peak in silver-sheathed $(Pb,Bi)_2Sr_2Ca_2Cu_3O_{10+y}$ tapes

K.-H. Müller and C. Andrikidis
Commonwealth Scientific and Industrial Research Organization, Division of Telecommunication and Industrial Physics, Lindfield, Australia 2070

Y. C. Guo
Centre for Superconducting and Electronic Materials, University of Wollongong, Australia 2522
(Received 1 May 1996; revised manuscript received 12 September 1996)

We have measured under zero-field-cooled (ZFC) and field-cooled (FC) conditions the magnetic moments of a high-quality $(Pb,Bi)_2Sr_2Ca_2Cu_3O_{10+y}$ tape at 5 K in perpendicular applied fields up to 1 T using a superconducting quantum interference device magnetometer. The intergranular magnetic moment, obtained by subtracting from the total magnetic moment the intragranular moment of the ''bent'' tape shows a pronounced anomalous peak at a positive field H_p. To interpret the experimental data the critical-state model for a flat superconducting strip in a perpendicular field is employed. The model includes the field dependence of the intergranular critical current density in first order. The field at grain-boundary Josephson junctions, which strongly influences the intergranular current, is estimated by taking the demagnetizing effect of the grains into account. The model predicts correctly the measured intergranular magnetic moments and the behavior of the anomalous peak in both the ZFC and the FC case. The saturation of the remanent intragranular magnetization occurs at a lower maximum field than the saturation of H_p which can be well understood in terms of the demagnetizing effect of the grains. A model which neglects grain demagnetization but instead takes the vortex distribution of vortices near Josephson junctions into account cannot describe quantitatively the observed behavior of the anomalous peak. [S0163-1829(97)02701-X]

I. INTRODUCTION

Silver-sheathed $(Pb,Bi)_2Sr_2Ca_2Cu_3O_{10+y}$ tapes (PBSCCO tapes) consist of thin, about 10 μm wide grain platelets where the platelets generally align within 5°–10° with the c direction perpendicular to the plane of the tape and the a and b directions are oriented at random from platelet to platelet.[1] This grain alignment in conjunction with a high density gives the tape a very high intergranular (transport) critical current density J_{cJ}. Measuring the magnetic moment of a tape, one finds that it consists of two parts, the intergranular moment, originating from an induced intergranular (transport) current and the intragranular magnetic moment, originating from induced currents circulating in grains.[2,3] In most PBSCCO tapes the intergranular magnetic moment is greater than the intragranular one simply because of the large intergranular critical current density J_{cJ}. This is contrary to non-grain-aligned polycrystalline high-temperature superconductors where, because of the small intergranular critical current density in these materials, the intergranular moment is much weaker than the intragranular one. As in non-grain-aligned polycrystalline high-temperature superconductors,[4–9] the transport critical current of PBSCCO tapes shows hysteretic behavior[10] which is attributed to the presence of trapped flux in the grains. Using the electrical four-point-probe method one finds that, because of the grain-boundary weak links, the critical current density decreases rapidly in an increasing applied field.[11] In the zero-field-cooling (ZFC) case, if one stops the field sweep at a maximum field H_m which is greater than H_{c1G} (lower critical field of the grains) and then decreases the applied field, one finds J_{cJ} to be greater than the initial, virgin critical current density and J_{cJ} goes through a maximum at a positive field H_p.[4–10] In the field-cooling (FC) case one finds a similar behavior for J_{cJ} but now $H_{p,\mathrm{FC}} \geqslant H_{p,\mathrm{ZFC}}$ because of the different amounts of flux trapped under FC and ZFC conditions.[7] The hysteretic behavior of J_{cJ} is most pronounced at low temperature. Because J_{cJ} is large in the PBSCCO tapes, the hysteretic behavior of J_{cJ} has a strong effect on the shape of the magnetic moment m. In good tapes, where the intergranular magnetic moment is larger than the intragranular one, a pronounced anomalous peak appears at a positive applied field which, according to the critical-state model, corresponds to the peak behavior of J_{cJ}.[2,12–14]

Evetts and Glowacki[4] have interpreted the hysteretic behavior of J_{cJ} in the ZFC case in a qualitative way by applying the critical-state model to the grains, arguing that the resulting dipole field of the grains, which spills into the intergranular region, causes the observed hysteresis. Quite a different model has been proposed by D'yachenko[9] in which the hysteretic behavior of J_{cJ} is assumed to be caused by the change in the direction of the intragranular current near the grain surface where the current adds to—or subtracts from—the Meissner shielding current, depending on whether the applied field is being increased or decreased.

We employ a simple theoretical model whose main features were initially proposed by Zhukov *et al.*[6] It strongly relates to the idea of the qualitative Evetts model which has been extended to explain quantitatively the hysteretic behavior of J_{cJ} in non-grain-aligned polycrystalline high-temperature superconductors.[7,8] The model used in this paper is based on the demagnetizing effect of the grains which affects the magnetic field that threads the grain-boundary Josephson junction. In the model the demagnetization depends

on the irreversible magnetization of the grains which in turn causes the critical current density to become irreversible resulting in the appearance of an anomalous peak in the intergranular magnetic moment.

In Sec. II we briefly describe the experiment to measure the intergranular and intragranular magnetic moments as a function of a magnetic field, applied perpendicular to the tape. In Sec. III we discuss the equations which describe the intergranular magnetic moment of the PBSCCO tape in a perpendicular magnetic field and introduce the demagnetizing effect of grains into the model. In Sec. IV we compare the experimental data of the intergranular magnetic moment with the predictions of our theoretical model and elucidate the dependence of the anomalous peak on the maximum applied field for both ZFC and FC conditions. We demonstrate that the demagnetizing effect of the grains is responsible for the observed behavior of the anomalous peak seen in the intergranular magnetic moment of PBSCCO tapes and we show that the D'yachenko model[9] cannot describe quantitatively the behavior of the anomalous peak.

Finally in Sec. V we summarize our findings. In the Appendix we derive equations for the anomalous peak using the D'yachenko model.

II. EXPERIMENT

The monofilamentary tape, used in our measurements, was prepared by employing the powder-in-tube method where strong alignment of the grains is achieved by pressing and rolling of the PBSCCO powder encapsulated in a silver sheath. Details about this method have been reported in Ref. 15. X-ray-diffraction measurements indicated that the core of the tape consisted of almost pure 2223 phase with only very small amounts of 2212 phase present. Using a four-point-probe method, with the usual 1 μV/cm electric-field criterion, the transport critical current density was found to be 16 000 A/cm^2 at 77 K in zero applied field. The average thickness of the superconducting core was 60 μm and the width of the core was about 2.3 mm. Two pieces of equal length of 5.8 mm were cut from a longer tape. The second piece was severely curled (bent) along its rolling direction to the small diameter of $\sim$1.2 mm and finally straightened. A commercial Quantum Design superconducting quantum interference device (SQUID) magnetometer was employed to measure the magnetic moments of the two pieces of the tape, the ''intact'' tape and the ''bent'' one, at 5 K under both zero-field-cooled (ZFC) and field-cooled (FC) conditions. The field was applied perpendicular to the tape surface, i.e., parallel to the crystallographic c direction of the grains. A 5-cm scan was used and the magnetic field was swept in the no-overshoot mode from the maximum field H_m to $-H_m$ with $\mu_0 H_m$ between 25 mT and 1 T.

III. THEORETICAL MODEL

A PBSCCO tape can be viewed as a grain network where the grains are well linked by grain-boundary Josephson junctions. The current density, $\mathbf{J}(\mathbf{r})$ at point $\mathbf{r}$ inside the tape can be split into two parts, the intergranular current density $\mathbf{J}_J(\mathbf{r})$ and the intragranular current density $\mathbf{J}_G(\mathbf{r})$ where

$$\mathbf{J}(\mathbf{r})=\mathbf{J}_J(\mathbf{r})+\mathbf{J}_G(\mathbf{r}). \tag{1}$$

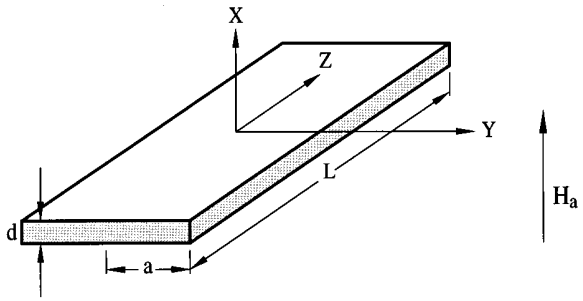

FIG. 1. Superconducting core of the monofilamentary tape approximated by a thin superconducting strip of thickness d, half width a, and length L.

The intergranular current is the Josephson current (thus the subscript J) flowing across grain boundaries while the intragranular current is flowing inside grains (thus the subscript G) and is determined by the pinning of pancake vortices in the grains.[2,16] By averaging the microscopic intergranular current density $\mathbf{J}_J(\mathbf{r})$ over a volume large compared to the grain size but small compared to the dimensions of the tape, one obtains the transport current density $\langle \mathbf{J}_J\rangle(\mathbf{r})$ which flows over the entire tape.

It has been shown by Majhofer and co-workers[17,18] that the critical current J_{cJ} of a Josephson network is determined not only by the magnitude of the Josephson critical current but also by the inductances of the Josephson-junction loops, formed by adjacent grains. Majhofer and co-workers[17,18] also showed that the magnetic-field behavior of the Josephson network can be described in terms of a critical-state model where the magnetic field penetrates the sample in a ''Bean-like'' fashion. Tinkham and Lobb[19] demonstrated that besides intrinsic pinning, which is inherent to a Josephson array, disorder, and defect pinning are of importance.

The transport current density distribution $\langle J_J\rangle$ which is induced in a superconducting strip (or tape), where the magnetic field H_a is applied perpendicular to the strip, has been calculated by Brandt and Indenbom[20] and later by Zeldov *et al.*[21]

In the zero-field-cooled case (ZFC), the induced transport current density $\langle J_{J\downarrow}\rangle$ which is flowing along the positive and negative z direction (see Fig. 1) when the applied field H_a is decreased ($\downarrow$) from the maximum applied field H_m to H_a, is given by

$$\langle J_{J\downarrow}\rangle(y,\mathrm{ZFC})=\langle J_J\rangle(y,H_m,J_{cJ})-\langle J_J\rangle(y,H_m-H_a,2J_{cJ}), \tag{2}$$

where

$$\langle J_J\rangle(y,H_a,J_{cJ})=\begin{cases}\dfrac{2J_{cJ}}{\pi}\arctan\dfrac{cy}{\sqrt{b^2-y^2}}; & |y|\leqslant b\\ J_{cJ}; & b<|y|<a\end{cases} \tag{3}$$

with

$$c=\frac{\sqrt{a^2-b^2}}{a},\quad b=\frac{a}{\cosh(H_a/H_d)}\quad\text{and}\quad H_d=J_{cJ}d/\pi. \tag{4}$$

Here, a is the half width and d is the thickness of the tape as indicated in Fig. 1. J_{cJ} is the field-independent intergranular critical current density where $|\langle J_J\rangle(y)|\leqslant J_{cJ}$.

In the field-cooled case (FC) we find

$$\langle J_{J\downarrow}\rangle(y,\mathrm{FC})=-\langle J_J\rangle(y,H_m-H_a,J_{cJ}). \tag{5}$$

Notice that here the last argument of $\langle J_J\rangle$ is J_{cJ} and not $2J_{cJ}$ as in Eq. (2). From the current density distribution $\langle J_{J\downarrow}\rangle(y)$ the intergranular magnetic field $H_{J\downarrow}(y)$ in x direction can be calculated using Biot-Savart's law. To an accuracy of d/a one finds[20]

$$H_{J\downarrow}(y)=\frac{d}{2\pi}\int_{-a}^{a}\frac{\langle J_{J\downarrow}\rangle(u)du}{y-u}+H_a. \tag{6}$$

When the applied field is decreased from H_m to H_a one obtains for the ZFC case

$$H_{J\downarrow}(y,\mathrm{ZFC})=H_J(y,H_m,J_{cJ})-H_J(y,H_m-H_a,2J_{cJ}), \tag{7}$$

where

$$H_J(y)=\begin{cases}0; & |y|\leqslant b\\ H_d\,\mathrm{arctanh}\,\dfrac{\sqrt{y^2-b^2}}{c|y|}; & b<|y|<a\\ H_d\,\mathrm{arctanh}\,\dfrac{c|y|}{\sqrt{y^2-b^2}}; & |y|<a.\end{cases} \tag{8}$$

And in the FC case we obtain

$$H_{J\downarrow}(y,\mathrm{FC})=H_m-H_J(y,H_m-H_a,J_{cJ}). \tag{9}$$

Notice that the second term on the right contains J_{cJ} and not $2J_{cJ}$ like the second term in Eq. (7).

To derive the above analytical expressions for $\langle J_{J\downarrow}\rangle$ it was assumed that J_{cJ} is independent of the magnetic field $H_{J\downarrow}$ inside the superconductor. This is an oversimplifying assumption, as the transport current of a Josephson network generally decreases monotonically in an increasing magnetic field. By taking the field dependence of the current density into account one obtains an improved description of the magnetic properties of the Bi-2223 tape, as we shall see below. It is of great importance to notice that the field at a grain-boundary Josephson junction does not only depend on the intergranular magnetic field $H_{J\downarrow}$, but also on the magnetic field generated by the grains adjacent to that junction.[4,6–8] Therefore, in addition to the intergranular magnetic field, field lines originating from grains thread the junction. The main idea of this paper is that the field H_i at a grain boundary can be approximated by

$$H_i=H_{J\downarrow}-\Gamma M_G(H_i,H_{im}), \tag{10}$$

which is an implicit equation for H_i, where the second term on the right is the contribution to the magnetic field from the grains. Here, Γ is the average demagnetizing factor of the grain network and M_G the average grain magnetization. The field H_{im} is the maximum field that was present at a grain boundary before the applied field was decreased and H_{im} is defined by the equation

$$H_{im}=H_{J\downarrow}(H_a=H_m)-\Gamma M_G(H_{im},H_{im}). \tag{11}$$

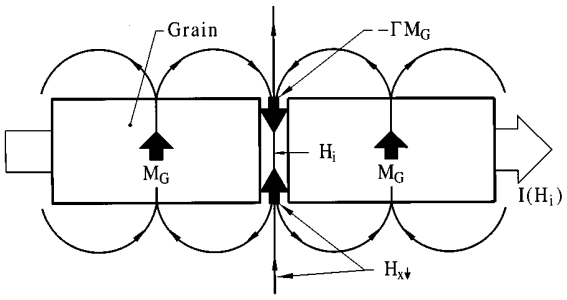

FIG. 2. Schematic of magnetic fields at a grain boundary.

Because the grain magnetization M_G is irreversible, H_i is hysteretic and thus the transport current of the tape, which is determined by Josephson currents, shows hysteretic behavior. The essence of the above described model is illustrated in Fig. 2 which shows schematically two grains where the intergranular current $I(H_i)$ crosses the grain boundary. The field H_i between the grains is composed of the intergranular field $H_{x\downarrow}(y)$ and the return-field, $-\Gamma M_G$, of the grains.

Equation (10) is an exact expression for a homogeneously magnetized, isolated ellipsoid in an external field of size $H_{J\downarrow}$ where the field H_i is the magnetic field inside the ellipsoid with the tangential component of H_i being steady at the surface.[22] The case of two spherical grains close together has been discussed by Waysand,[23] while more complicated configurations of grains have been investigated by Hodgdon, Navarro, and Campbell,[24] where in addition comparisons with the effective mean-field theory were made. An attempt to estimate Γ, using the magnetic dipole approximation, has been made by Altshuler.[8] In reality the demagnetization factor will vary from one grain boundary to the next and thus the factor Γ in Eq. (10) is meant to be an average of the demagnetizing factors of the grain network.

To correct in first order for the missing field dependence of J_{cJ}, we introduce the revised current density $\langle\tilde{J}_{J\downarrow}\rangle$ to calculate the intergranular magnetic moment $m_{J\downarrow}$ where

$$\langle\tilde{J}_{J\downarrow}\rangle=\langle J_{J\downarrow}\rangle\frac{H_0^n}{(H_0+|H_i|)^n}. \tag{12}$$

Notice that $\langle\tilde{J}_{J\downarrow}\rangle$ depends on H_i and not on $H_{J\downarrow}$ which accounts for the demagnetizing effect of grains and that $H_{J\downarrow}$ in Eq. (10) is calculated using $\langle J_{J\downarrow}\rangle$ and not $\langle\tilde{J}_{J\downarrow}\rangle$ which makes it a first-order correction scheme to include the field dependence of the intergranular critical current density into the model. The exponent n and the field H_0 depend on the type of Josephson junctions[25] and the morphology of the network[18,19] and both n and H_0 are treated here as phenomenological parameters.

For the grain magnetization M_G we adopted the simple expressions derived from the Bean model[26,27] for an infinite slab of thickness $2R_G$, where R_G corresponds to the average grain radius, in a parallel field. The Bean model assumes that the critical current density of grains, J_{cG}, is field independent and $H_{c1G}=0$. One finds for decreasing H_i in the ZFC case

$$M_G^{\mathrm{ZFC}}=\begin{cases}\dfrac{H_{im}^2}{2H^*}-\dfrac{(H_i-H_{im})^2}{4H^*}-H_i; & H_{im}<H^* \\ H_{im}-\dfrac{H^*}{2}-\dfrac{(H_i-H_{im})^2}{4H^*}-H_i; & H_{im}-2H^*\leqslant H_i \\ \dfrac{H^*}{2}; & H_i<H_{im}-2H^*.\end{cases} \tag{13}$$

Here, H^* is the field of full penetration into grains, i.e., $H^*=J_{cG}R_G$.

In the FC case one finds[28]

$$M_G^{\mathrm{FC}}=\begin{cases}H_{im}-H_i-\dfrac{(H_{im}-H_i)^2}{2H^*}-H_i; & H_{im}-H_i\leqslant H^* \\ \dfrac{H^*}{2}; & H_{im}-H_i>H^*\ .\end{cases} \tag{14}$$

Figures 3(a) and 3(b) show a schematic drawing of H_i versus $H_{J\downarrow}$ for the ZFC and FC cases, respectively, using Eq. (10). As can be seen, when $H_{J\downarrow}$ decreases, the field H_i becomes zero at $H_{J\downarrow}=H_p>0$ where $H_{p,\mathrm{FC}}\geqslant H_{p,\mathrm{ZFC}}$. According to Eq. (12), the transport current $\langle J_{J\downarrow}\rangle$ reaches its maximum at H_p.

Figure 4 shows the field distributions $H_{J\downarrow}$ and H_i as a function of y across the superconducting tape. Because the applied field is perpendicular to the surface of the tape, the field near the edges reaches values greater than H_m. The values for H_i can differ significantly from $H_{J\downarrow}$, indicating the importance of the grain demagnetizing effect.

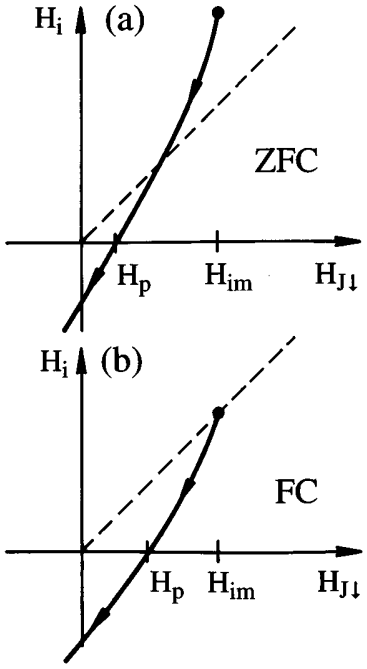

FIG. 3. Schematic of the field H_i at a grain boundary due to the demagnetizing effect of adjacent grains as a function of the decreasing intergranular magnetic field $H_{J\downarrow}$ for (a) ZFC condition and (b) FC condition. H_{im} is the maximum field at a grain boundary.

The total magnetic moment **m** is defined as

$$\mathbf{m}=\frac{1}{2}\int \mathbf{r}\times\mathbf{J}(\mathbf{r})d^3r. \tag{15}$$

For a superconducting tape in perpendicular field H_a, where H_a was set by decreasing the applied field from H_m to H_a, one obtains for the intergranular magnetic moment[20,2]

$$m_{J\downarrow}=2Ld\int_0^a y\tilde{J}_{J\downarrow}(y)dy. \tag{16}$$

The magnetic field H_p, where the intergranular magnetic-moment m_J peaks, as a function of the maximum applied field H_m, can be determined from calculations of the magnetic-moment loops $m_J(H_a,H_m)$.

Instead of doing a lengthy calculation for H_p using Eqs. (2)–(16), one can get an approximate value for H_p in the case of $H_m\gg H_d$ by using Eq. (10) with $H_i=0$ and $H_{J\downarrow}=H_p$ which results in

$$H_p\simeq\Gamma M_G[H_i=0,H_{im}(H_m)]. \tag{17}$$

Because M_G saturates at large H_m, the peak field H_p also saturates and it is thus useful to compare the saturation of H_p with the saturation of the remanent intragranular magnetization M_G^R of the grains. The remanent intragranular magnetization M_G^R is defined by Eq. (10) for $H_{J\downarrow}=0$ which gives

$$H_i^R=-\Gamma M_G(H_i^R,H_{im}). \tag{18}$$

Thus

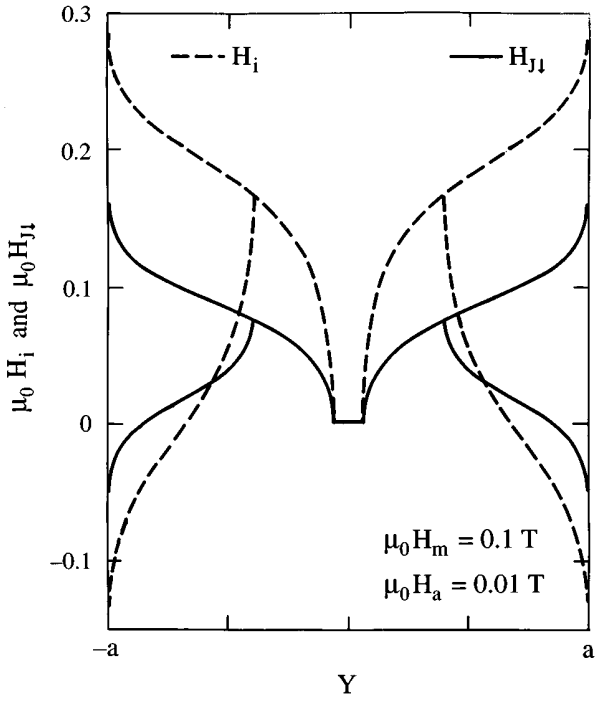

FIG. 4. Calculated intergranular magnetic field $H_{J\downarrow}$ and magnetic field H_i at grain boundaries as a function of the position y along the width of the superconducting core of the tape for a maximum field of $\mu_0H_m=0.1$ T and an applied field $\mu_0H_m=0.01$ T.

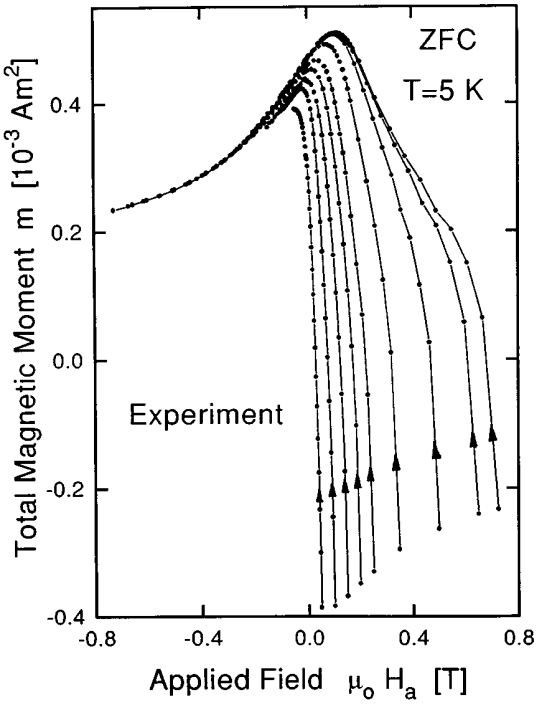

FIG. 5. Measured total magnetic moment $m_{\downarrow}$ (intact tape) under ZFC conditions at 5 K versus the applied magnetic field H_a for different maximum fields H_m. The applied field, after an initial increase from 0 to H_m, is decreased from H_m to $-H_m$.

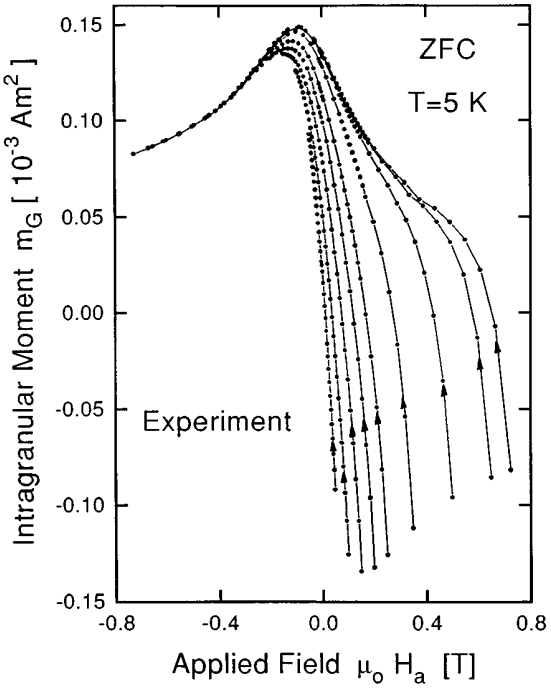

FIG. 6. Measured intragranular magnetic moment $m_{G\downarrow}$ (bent tape) under ZFC conditions at 5 K versus the applied magnetic field H_a for different maximum fields H_m. The applied field, after an initial increase from 0 to H_m, is decreased from H_m to $-H_m$.

$$M_G^R \equiv M_G(H_i^R, H_{im}). \tag{19}$$

Notice that when measuring the intragranular magnetization no intergranular current is present and $H_{J\downarrow}=H_a$. In the limit of $\Gamma\to 0$, both H_p and M_G^R saturate in the same fashion which will be illustrated later in Figs. 16 and 17.

The model described above [Eqs. (10)–(14)] is essentially a mathematical formulation of the qualitative Evetts model.[4] Our model goes beyond the Evetts model as it takes into account the effect of the magnetic field which is generated by the intergranular current. While in this work the anomalous peak in the magnetic moment of a PBSCCO tape is investigated, Evetts and Glowacki[4] measured the irreversible critical current density as a function of the applied field using the electrical four-point-probe method. This irreversible critical current density is given by Eq. (12) with $\langle J_{J\downarrow}\rangle = J_c$. A model for the irreversible critical current based on Eqs. (10) and (12) has been reported in Ref. 7.

IV. RESULTS AND DISCUSSION

Figure 5 shows the measured ZFC total magnetic moment $m_{\downarrow}$ of the ''intact'' tape at 5 K for a decreasing applied field H_a where the maximum applied fields are $\mu_0 H_m = 0.05$, 0.1, 0.15, 0.2, 0.25, 0.35, 0.5, 0.65, and 0.725 T. The magnetic moment $m_{\uparrow}$ for an increasing applied field is simply given by $m_{\uparrow}(H_a, H_m) = -m_{\downarrow}(-H_a, H_m)$ and is therefore not shown. The most striking feature of Fig. 5 is the anomalous peak positioned at a positive applied field while commonly superconductors show a peak in the magnetic moment at a negative applied field. The virgin part of the magnetic moment is not shown for clarity.

Figure 6 shows the measured ZFC intragranular magnetic moment $m_{G\downarrow}$ of the ''bent'' tape for different values of H_m. The intragranular magnetization shows, as expected, a peak at a negative applied field which shifts slightly to less negative fields with increasing maximum field H_m. The origin of this intragranular peak is well understood in terms of a critical state model in which the intragranular critical current density is field dependent and decreases monotonically with increasing field. Figure 6 reveals that roughly 25% of the total magnetic moment originates from currents induced in the grains. The question that arises here is whether the so-called intragranular magnetic moment is indeed only been caused by currents flowing in grains and not by currents flowing in larger grain clusters. To answer this question we have studied in Ref. 2 the remanent magnetic moment of the tape as a function of the degree of bending and in Ref. 13 we crushed the tape and carefully scraped the core material out of the silver cladding and measured its magnetic moment. The investigations revealed that the magnetic moment of a strongly bent tape is that of the grains and that the contribution from grain clusters, in which the intergranular current is flowing, is negligibly small.

Figure 7 displays the measured intergranular ZFC magnetic moment $m_{J\downarrow}$, obtained by subtracting from the data of Fig. 5 the data of Fig. 6 where $m_{J\downarrow} = m_{\downarrow} - m_{G\downarrow}$. The anomalous peak is even more pronounced than in the case of the intact tape. The inset in Fig. 7 shows more clearly the evolution of the anomalous peak as a function of the maximum field H_m.

The calculated intergranular ZFC magnetic moment $m_{J\downarrow}$,

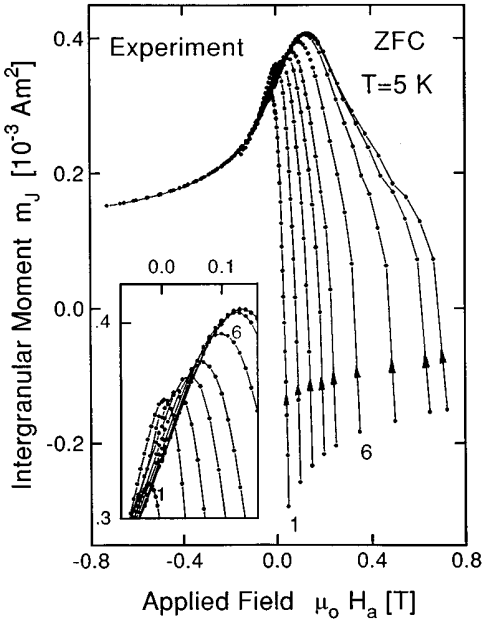

FIG. 7. Measured intergranular magnetic moment $m_{J\downarrow}$ under ZFC conditions at 5 K versus the applied magnetic field H_a for different maximum fields H_m. The applied field, after an initial increase from 0 to H_m, is decreased from H_m to $-H_m$. The inset shows the evolution of the anomalous peak for different maximum fields H_m.

using the model developed in this paper [Eqs. (2)–(16)], is displayed in Fig. 8. The parameters used are $d=60$ μm, $a=1.1$ mm, $n=2$, $\mu_0 H_0=1$ T, $J_c=1.2\times10^9$ A m^{-2}, $\mu_0 H^*=0.38$ T, and $\Gamma=0.7$. The calculated moment $m_{J\downarrow}$

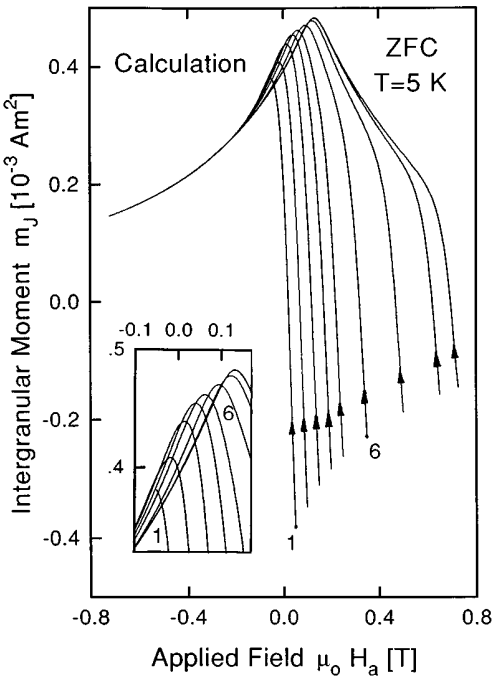

FIG. 8. Calculated intergranular magnetic moment $m_{J\downarrow}$ under ZFC conditions at 5 K versus the applied magnetic field H_a for different maximum fields H_m. The inset shows the evolution of the anomalous peak for different maximum applied fields H_m.

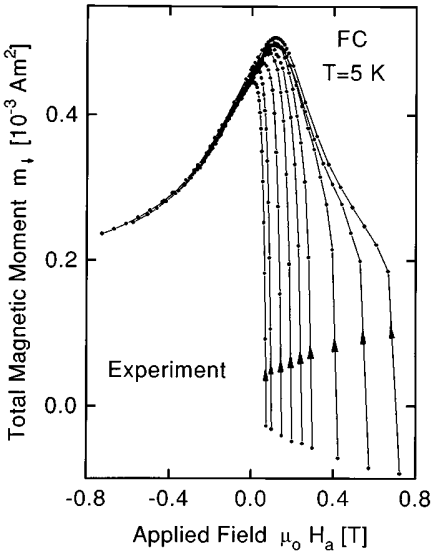

FIG. 9. Measured total magnetic moment $m_{\downarrow}$ (intact tape) under FC conditions at 5 K versus the applied magnetic field H_a for different maximum fields H_m. The applied field is decreased from H_m to $-H_m$.

shows excellent resemblance with the experimental data of Fig. 7 and the evolution of the anomalous peak for increasing H_m is well reproduced.

Figure 9 shows the measured FC total magnetic moment $m_{\downarrow}$ of the intact tape at 5 K for a decreasing applied field H_a at $\mu_0 H_m=0.075$, 0.1, 0.15, 0.2, 0.25, 0.3, 0.425, 0.575, and 0.725 T. The FC magnetic moment $m_{J\downarrow}$ at $H_a=H_m$ has a value close to zero which is different to the ZFC case in Fig. 5 as more flux penetrates the sample at $H_a=H_m$ in the FC case than the in the ZFC one. Like under the ZFC condition, an anomalous peak appears at a positive field.

Figure 10 shows the measured intragranular magnetic moment $m_{G\downarrow}$ of the bent tape. Like in the ZFC case, the peak in the intragranular magnetic moment appears at negative applied fields. There is a clear difference between the magnitudes of the ZFC and the FC intragranular magnetic moments at $H_a=H_m$. Figure 10 reveals that roughly 25% of the total magnetic moment originates from currents induced in the grains.

Figure 11 displays the measured intergranular FC magnetic moment $m_{J\downarrow}$ where $m_{J\downarrow}=m_{\downarrow}-m_{G\downarrow}$. The inset shows the anomalous peak for different H_m in greater detail.

Figure 12 shows the calculated intergranular FC magnetic moment $m_{J\downarrow}$ using the model developed in this paper [Eqs. (2)–(16)]. The parameters used are the ones used to calculate the ZFC intergranular magnetic moment in Fig. 8. There is a strong resemblance to the experimental data of Fig. 11 and, as indicated in the inset, the evolution of the anomalous peak for increasing H_m is reasonably well reproduced.

Figure 13 compares the measured $H_p(H_m)$ data with the measured intragranular remanent magnetic moment $m_G^R(H_m)=m_{G\downarrow}(H_a=0,H_m)$ for the ZFC case, respectively. The remanent intragranular magnetic moment m_G^R saturates before saturation of H_p occurs and both curves are shifted with respect to the H_m axis by about 0.1 T.

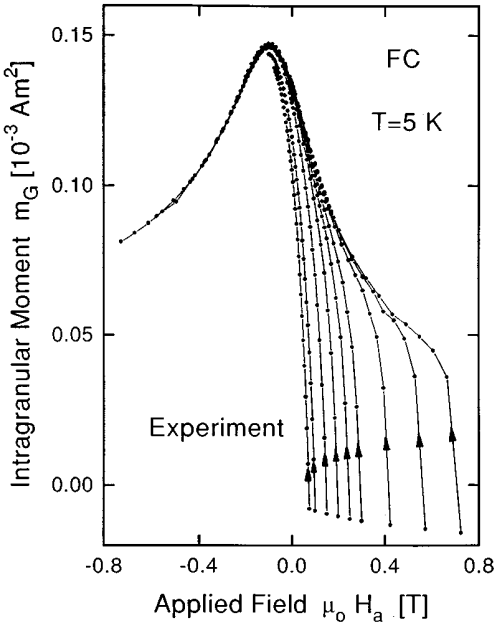

FIG. 10. Measured intragranular magnetic moment $m_{G\downarrow}$ (bent tape) under FC conditions at 5 K versus the applied magnetic field H_a for different maximum fields H_m. The applied field is decreased from H_m to $-H_m$.

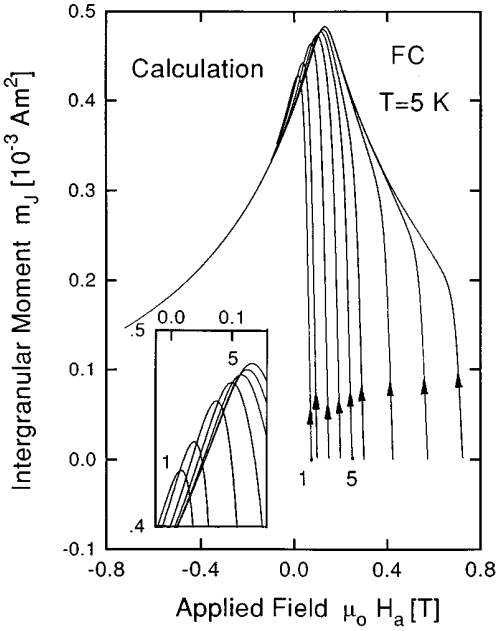

FIG. 12. Calculated intergranular magnetic moment $m_{J\downarrow}$ under FC conditions at 5 K versus the applied magnetic field H_a for different maximum fields H_m. The inset shows the evolution of the anomalous peak for different maximum applied fields H_m.

Figure 14 shows the calculated values of H_p and m_G^R versus H_m which agrees reasonably well with the experimental data of Fig. 13. The anomalous peak field H_p was calculated by using Eqs. (2)–(16) and H_p was determined numerically by calculating where $m_{J\downarrow}$ peaks. To calculate m_G^R Eqs. (18) and (19) with $\Gamma=0.7$ were used, where $m_G^R = 2adLM_G^R$.

Figures 15 and 16 display experimental data and calculations of H_p and m_G^R versus H_m in the FC case. As can be seen, in the FC case, H_p saturates at about $\mu_0 H_m = 0.4$ T,

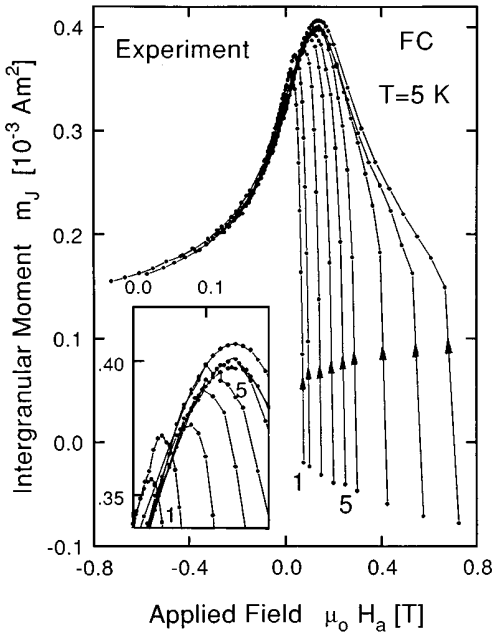

FIG. 11. Measured intergranular magnetic moment $m_{J\downarrow}$ under FC conditions at 5 K versus the applied magnetic field H_a for different maximum fields H_m. The applied field is decreased from H_m to $-H_m$. The inset shows the evolution of the anomalous peak for different maximum applied fields H_m.

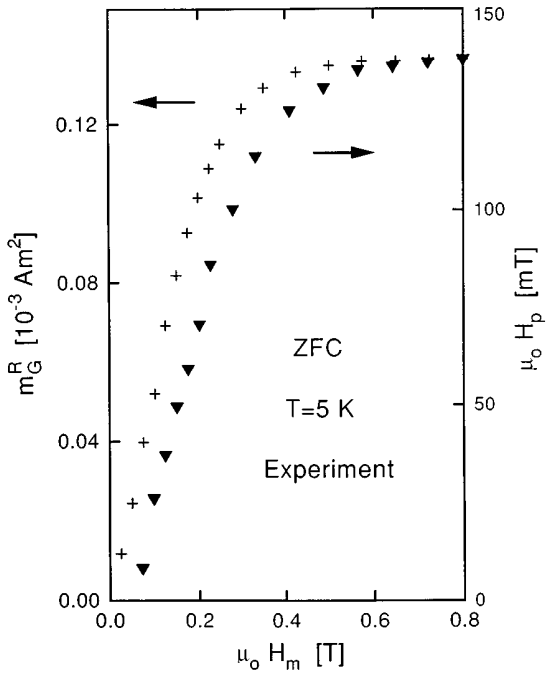

FIG. 13. Measured intragranular remanent magnetic moment m_G^R and the measured anomalous peak field H_p at 5 K under ZFC conditions as a function of the maximum applied field H_m.

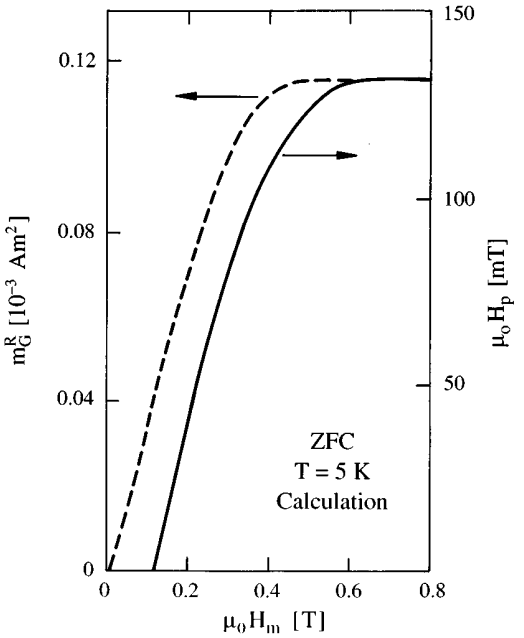

FIG. 14. Calculated intergranular remanent magnetic moment m_G^R and the calculated anomalous peak field H_p at 5 K under ZFC conditions as a function of the maximum applied field H_m.

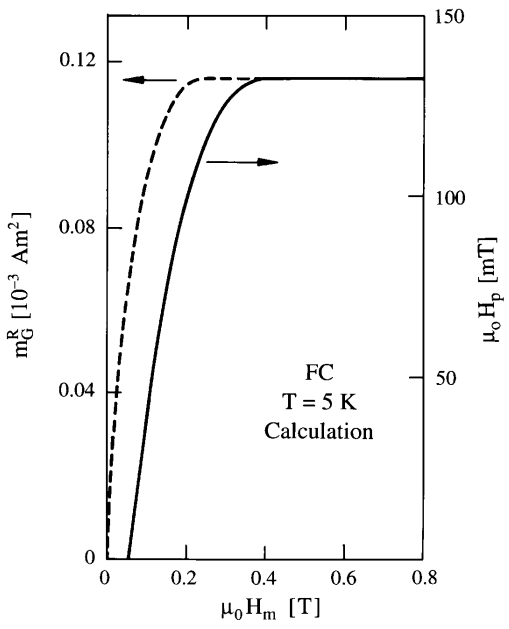

FIG. 16. Calculated intergranular remanent magnetic moment m_G^R and the measured anomalous peak field H_p at 5 K under FC conditions as a function of the maximum applied field H_m.

while in the ZFC case (Fig. 13), H_p saturates at about $\mu_0 H_m = 0.6$ T.

Figures 17 and 18 show the calculated ZFC and FC remanent magnetization $M_G^R(H_m)$ as defined by Eqs. (18) and (19) and the peak field $H_p(H_m)$ approximated by Eq. (17) for $\Gamma = 1/3$ and $\Gamma = 1$. The difference in the saturation of M_G^R (or m_G^R) and H_p is caused by the demagnetizing effect of the grains. In the limit $\Gamma \to 0$ both m_G^R and H_p saturate in the same fashion. Thus, the relative displacement of the curves for $m_G^R(H_m)$ and $H_p(H_m)$ is a direct measure of the average demagnetizing factor Γ. Here, $H_p = 0$ at $H_m = 0$ which is different than the full calculations presented in Figs. 14 and 16, indicating that Eq. (17) can only be used when $H_m \gg H_d$.

We also have measured H_p and m_G^R for $\mu_0 H_m = 5$ T and found that $H_p(5\text{ T}) = H_p(0.8\text{ T})$ and $m_G^R(5\text{ T}) = m_G^R(0.8\text{ T})$ as expected. It is certainly of interest to investigate the depen-

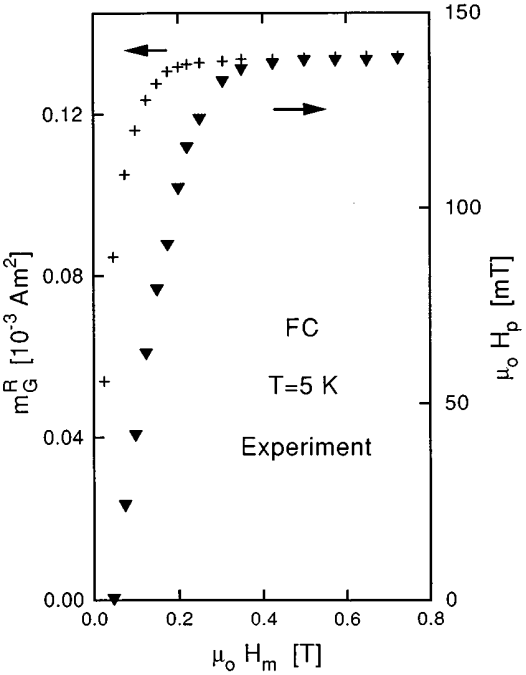

FIG. 15. Measured intragranular remanent magnetic moment m_G^R and the measured anomalous peak field H_p at 5 K under FC conditions as a function of the maximum applied field H_m.

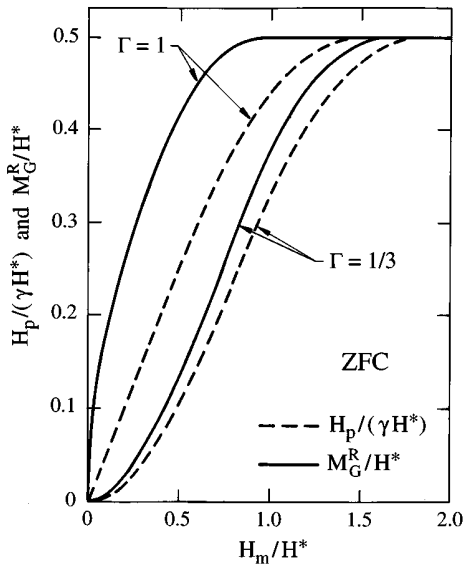

FIG. 17. Calculated values of $H_p/(\Gamma H^*)$ and M_G^R/H^* versus H_m/H^* for two different demagnetizing factors Γ under ZFC conditions using Eqs. (17)–(19).

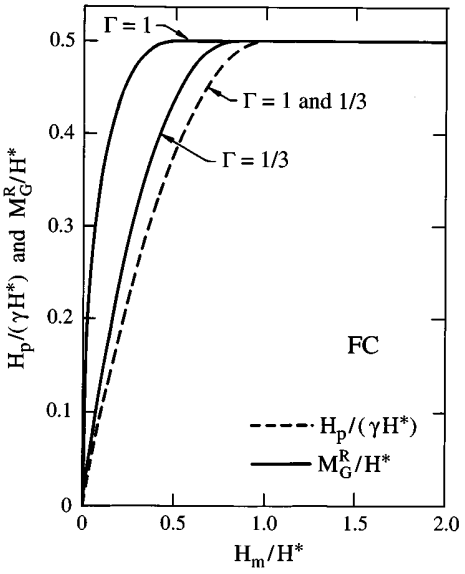

FIG. 18. Calculated values of $H_p/(\Gamma H^*)$ and M_G^R/H^* versus H_m/H^* for two different demagnetizing factors Γ under FC conditions using Eqs. (17)–(19).

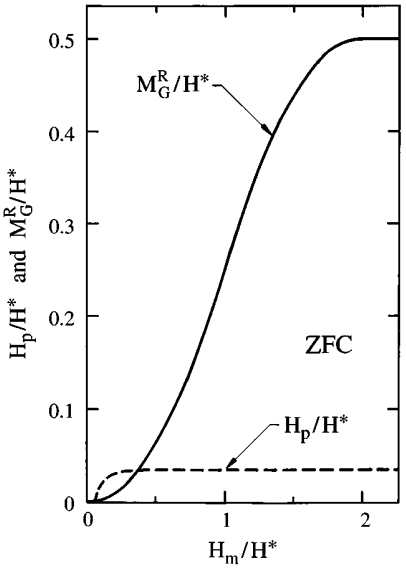

FIG. 19. Calculated normalized anomalous peak field H_p/H^* in the D'yachenko model and the calculated normalized remanent magnetization M_G^R/H^* versus the normalized maximum applied field H_m/H^* under ZFC conditions.

dence of H_p and m_G^R on grain size which has not been done in this paper.

The model, which is described in this paper, reveals that the demagnetizing effect of grains can be used to explain the anomalous peak in the intergranular magnetic moment of PBCCO tapes, caused by the irreversible behavior of the transport current. Besides the grain demagnetization, there seems to be another possible source for the irreversibility of the transport current as discussed by D'yachenko[9] and others. They studied the Josephson current behavior between two superconducting semi-infinite slabs which are in the mixed state with vortex pinning, where the applied field is parallel to the slabs. In the D'yachenko model the Josephson critical current density is

$$J_c^{\mathrm{Jos}} \sim \left| \frac{\sin(\pi\Phi/\Phi_0)}{\pi\Phi/\Phi_0} \right|, \tag{20}$$

where Φ_0 is the flux quantum and

$$\Phi \simeq 4\mu_0 R_G \lambda^2 J_s . \tag{21}$$

Here J_s is the current density at the surface of a grain at the grain boundary and λ is the London penetration depth of the grains, ignoring the anisotropy of $\lambda(\lambda_c \neq \lambda_{ab})$. If $R_G \gg \lambda$ and if the field H_a, which threads the junction, is large compared to $R_G J_{cG}$, one finds

$$J_s \simeq J_M \pm J_{cG} , \tag{22}$$

where J_M is the Meissner shielding current density. The exact expression for Φ and J_s as a function of H_a and H_m are given in the Appendix. The $\pm$ signs in Eq. (22) are for an increasing and decreasing applied field, respectively, and cause the transport current to become irreversible.

In order to find out if the D'yachenko approach can account for our experimental data we have calculated the peak field H_p for both ZFC and FC conditions from $\Phi(H_p, H_m) = 0$ where $\Phi(H_p, H_m)$ is given in the Appendix.

Figure 19 shows for the ZFC case the normalized peak field H_p/H^* and the normalized remanent intragranular magnetization M_G^R/H^* as a function of the normalized maximum field H_m/H^* where $H^* = J_{cG} R_G$. Similar results are obtained for the FC case. For the average grain size along the a-b direction of Bi-2223 grains a value of $2R_G = 12$ μm was assumed and $\lambda = \lambda_{ab} = 0.2$ μm (Refs. 29 and 30) and $\mu_0 H_{c1G} = 0.015$ T. According to Fig. 19, independent of H^*, the D'yachenko model predicts $H_p(H_m \to \infty) \ll M_G^R(H_m \to \infty)$ which is contradictory to the experimental data where $H_p(H_m \to \infty) \simeq M_G^R(H_m \to \infty)$. Figure 19 also demonstrates that the D'yachenko model predicts that $H_p(H_m)$ saturates at a lower H_m than the intragranular magnetization M_G^R which is due to the fact that in the D'yachenko model the Josephson current is only influenced by vortices which are about λ away from the grain boundary and vortices located inside the grains do not affect the Josephson current. The experimental data in Figs. 13 and 15 show that M_R^G saturates at a lower maximum field H_m than the peak field H_p which is in contradiction with the D'yachenko model. Because of these discrepancies, we believe that the origin of the anomalous peak is less due to an irreversible surface current density J_s but instead mainly due to the demagnetizing effect of the grains. Despite this, the D'yachenko model seems be suitable to account for the sudden rise of J_{cJ} often observed in transport current measurements when decreasing the applied field slightly from its maximum value.[9]

V. CONCLUSIONS

We have measured the magnetic moments of a high-quality PBSCCO tape in perpendicular fields up to 1 T at 5 K using a SQUID magnetometer. Subtracting from the total magnetic moment of the intact tape the intragranular magnetic moment of the bent tape, the intergranular magnetic moment, which originates from an induced intergranular

(transport) current flowing over the entire tape, is obtained. The intergranular magnetic moment shows an anomalous peak in decreasing applied field at a positive field H_p. The anomalous peak reflects the irreversible behavior of the transport critical current density. We have modeled the intergranular magnetic moment as a function of the applied field at different maximum fields H_m by using a critical-state model for a thin superconducting strip in a perpendicular field. The model was extended to include the field dependence of the intergranular current in first order and the important demagnetizing effect of the grains, which modifies the field at grain-boundary Josephson junctions, was taken into account. Both ZFC and FC cases were studied. Because the intergranular critical current density depends on the field at the grain boundaries, the irreversibility of the grain magnetization causes the transport critical current density to become irreversible. The model presented in this paper is in excellent agreement with the measured intergranular magnetic moment versus decreasing applied field for different maximum applied fields H_m for both ZFC and FC cases. The shift of the anomalous peak field H_p with increasing H_m is correctly predicted by the model. The fact that H_p and the remanent magnetic moment m_G^R of the grains do not saturate at identical fields H_m can be well understood in terms of the demagnetizing effect of grains. The relative displacement of the $H_p(H_m)$ and $m_R^G(H_m)$ curves give a measure of the demagnetizing factor Γ of the grain network where $\Gamma=0.7$ was found for the PBSCCO tape investigated. The maximum peak shift is $H_p^{\max}=\Gamma M_G^R(H_m\to\infty)$ and therefore how pronounced the anomalous peak appears in the intergranular magnetic moment depends on the grain network morphology (Γ), the grain size ($2R_G$), and the flux pinning in grains (J_{cG}). It also depends on the field dependence of the intergranular current density $\langle\tilde{J}_{J\downarrow}\rangle$. If $H_p^{\max}$ is small and $\langle\tilde{J}_{J\downarrow}\rangle$ does not drop significantly in an applied field of size $H_p^{\max}$, the anomalous peak is difficult to detect. In high-quality PBSCCO tapes the intergranular magnetic moment is larger than the intragranular one and the anomalous peak is already clearly visible in the total magnetic moment of the intact tape. We also have shown that the D'ychenko model is unlikely to account quantitatively for the behavior of the anomalous peak of the intergranular magnetic moment in PBSCCO tapes.

ACKNOWLEDGMENTS

The authors gratefully acknowledge the support of Metal Manufactures Ltd., the Energy Research and Development Corporation, the Department of Industry Science and Technology, and the Australian Research Council.

APPENDIX

In order to evaluate the maximum Josephson current across a grain boundary in dependence on the flux trapped inside the two adjacent grains, the second Ginzburg-Landau equation[25] is used

$$\nabla\Theta_k=\frac{2\pi}{\Phi_0}\,(-\mu_0\lambda^2\mathbf{J}_k+\mathbf{A}), \tag{A1}$$

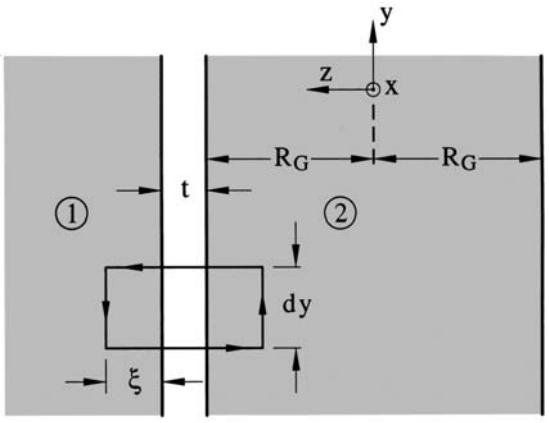

FIG. 20. The integration path across a grain boundary and parallel to the grain surface where the grains are represented by slabs of thickness $2R_g$.

where $k=1,2$ denotes the superconductors forming the junction, Θ_k is the phase of the order parameter in superconductor k, Φ_0 is the flux quantum, $\mathbf{J}_k$ is the current density inside the superconductor k, λ is the penetration depth (ignoring the anisotropy, $\lambda_c\neq\lambda_{ab}$), and $\mathbf{A}$ is the vector potential. Integrating both sides of Eq. (A1) along the path shown in Fig. 20, one obtains the relation[31,32]

$$\frac{d\varphi}{dy}=\frac{4\pi\mu_0}{\Phi_0}\,[(\xi+t/2)H_a+\lambda^2 J_s], \tag{A2}$$

where $\varphi=\Theta_1-\Theta_2-2\pi\int_1^2 dz A_z/\Phi_0$ is the gauge-invariant phase difference, H_a is the field inside the junction pointing in the x direction, ξ is the coherence length ($\xi\ll\lambda$), t is the spacing between the superconductors, and J_s is the current density at the surface which in superconductor 2 is positive when pointing into the y direction.

The current density, J_s, at the surface is given by

$$J_s=\frac{1}{\mu_0}\left.\frac{\partial B}{\partial z}\right|_{z=\xi+t/2\cong 0}. \tag{A3}$$

Representing the grains by two slabs of thickness $2R_G$, the magnetic induction B, pointing in the x direction inside the superconductors, can be determined using the inhomogeneous London equation

$$B(z)-\lambda^2\frac{\partial^2 B(z)}{\partial z^2}=\Phi_0 n(z). \tag{A4}$$

Here $n(z)$ is the flux density distribution of Abrikosov (pancake) vortices where the flux lines point in the x direction. The boundary conditions are $B(R_G)=B(-R_G)=\mu_0 H_a$, where we assume $H_{c1G}=0$. The solution of Eq. (A4) is

$$B(z)=\left[\mu_0 H_a-\frac{\Phi_0}{\lambda}\int_0^{R_G}d\eta\, n(\eta)\sinh\left(\frac{\eta-R_G}{\lambda}\right)\right]\times\frac{\cosh(z/\lambda)}{\cosh(R_G/\lambda)}+\frac{\Phi_0}{\lambda}\int_0^z d\eta\, n(\eta)\sinh\left(\frac{\eta-z}{\lambda}\right). \tag{A5}$$

With Eq. (A3) one obtains for J_s, using Eq. (A5)

$$J_s=\left[\frac{H_a}{\lambda}-\frac{\Phi_0}{\lambda^2\mu_0}\int_0^{R_G}d\eta\, n(\eta)\sinh\left(\frac{\eta-R_G}{\lambda}\right)\right]\tanh\left(\frac{R_G}{\lambda}\right)$$
$$-\frac{\Phi_0}{\lambda^2\mu_0}\int_0^{R_G}d\eta\, n(\eta)\cosh\left(\frac{\eta-R_G}{\lambda}\right). \quad \text{(A6)}$$

The Abrikosov vortex distribution, $n(z)$, inside the superconducting grains depends on the intragranular critical current density, J_{cG}. It is assumed that J_{cG} is independent of the local magnetic induction B (Bean model). The Abrikosov flux density, when unequal to zero, has the form[26,27]

$$n(z)=n(0)\pm\frac{\mu_0}{\Phi_0}J_{cG}z. \quad \text{(A7)}$$

In the following B_a and B_m are the inductances at the surface inside the superconductor where $B_a=\mu_0(H_a+M_{\rm eq})$ and $M_{\rm eq}$ is the equilibrium magnetization. For simplicity we use $M_{\rm eq}=-H_a$ for $0\leqslant H_a\leqslant H_{c1G}$ and $M_{\rm eq}=-H_{c1G}$ for $H_a>H_{c1G}$ where H_{c1G} is the lower critical field of the grains.

Under ZFC conditions one obtains (i) if $B_m\leqslant B^*=\mu_0J_{cG}R_G$,

$$\frac{J_s}{J_{cG}}=\left[\frac{H_a-B_a/\mu_0}{J_{cG}\lambda}-2\sinh\left(\frac{R_G}{\lambda}\frac{B_m-B_a}{2B^*}\right)+\sinh\left(\frac{R_G}{\lambda}\frac{B_m}{B^*}\right)\right]$$
$$\times\tanh\left(\frac{R_G}{\lambda}\right)-1+2\cosh\left(\frac{R_G}{\lambda}\frac{B_m-B_a}{2B^*}\right)$$
$$-\cosh\left(\frac{R_G}{\lambda}\frac{B_m}{B^*}\right), \quad \text{(A8)}$$

(ii) if $B_m>B^*$ and $B_m-2B^*\leqslant B_a\leqslant B_m$,

$$\frac{J_s}{J_{cG}}=\left[\frac{H_a-B_a/\mu_0}{J_{cG}\lambda}-2\sinh\left(\frac{R_G}{\lambda}\frac{B_m-B_a}{2B^*}\right)+\sinh\left(\frac{R_G}{\lambda}\right)\right]$$
$$\times\tanh\left(\frac{R_G}{\lambda}\right)-1+2\cosh\left(\frac{R_G}{\lambda}\frac{B_m-B_a}{2B^*}\right)-\cosh\left(\frac{R_G}{\lambda}\right), \quad \text{(A9)}$$

and (iii) if $B_m>B^*$ and $-B_m\leqslant B_a\leqslant B_m-2B^*$,

$$\frac{J_s}{J_{cG}}=\frac{H_a-B_a/\mu_0}{J_{cG}\lambda}\tanh\left(\frac{R_G}{\lambda}\right)-1+\frac{1}{\cosh(R_G/\lambda)}. \quad \text{(A10)}$$

It is interesting to note that J_s in Eq. (A10) is independent of B_m and that one obtains from Eq. (A10) for $B_a=0$ and $R_G\gg\lambda$ the result $H_p=(\lambda/R_G)H^*$.

Under FC conditions one obtains (i) if $B_m\leqslant B^*/2$,

$$\frac{J_s}{J_{cG}}=\left[\frac{H_a-B_a/\mu_0}{J_{cG}\lambda}+\frac{B_m}{\mu_0J_{cG}\lambda}\cosh\left(\frac{R_G}{\lambda}\right)\right.$$
$$\left.-\sinh\left(\frac{R_G}{\lambda}\frac{B_m-B_a}{B^*}\right)\right]\tanh\left(\frac{R_G}{\lambda}\right)-1$$
$$-\frac{B_m}{\mu_0J_{cG}\lambda}\sinh\left(\frac{R_G}{\lambda}\right)+\cosh\left(\frac{R_G}{\lambda}\frac{B_m-B_a}{B^*}\right) \quad \text{(A11)}$$

(ii) if $B_m>B^*/2$ and $B_m-B^*\leqslant B_a\leqslant B_m$ one obtains Eq. (A11) and if $-B_m\leqslant B_a<B_m-B^*$ one obtains Eq. (A10) as the magnetic field profiles for ZFC and FC become identical.

Because J_s is independent of y in the slab approximation, one obtains from Eq. (A2)

$$\varphi(y)=\frac{4\pi\mu_0}{\Phi_0}[(\xi+t/2)H_a+\lambda^2J_s]y+\varphi_0. \quad \text{(A12)}$$

The critical Josephson current density, $J_c^{\rm Jos}$, is given by determining the constant φ_0 which maximizes the current density, $J^{\rm GB}$, across a grain-boundary junction of width $2R_G$ where

$$J^{\rm GB}=\frac{J_0}{2R_G}\int_{-R_G}^{R_G}\sin\{4\pi\mu_0[(\xi+t/2)H_a+\lambda^2J_s]y/\Phi_0$$
$$+\varphi_0\}dy. \quad \text{(A13)}$$

J_0 is the Josephson current density if no flux is trapped inside grains and no field is applied. One finds

$$J_c^{\rm Jos}=J_0\left|\frac{\sin(\pi\Phi/\Phi_0)}{\pi\Phi/\Phi_0}\right|, \quad \text{(A14)}$$

where

$$\Phi(H_a,H_m)=4\mu_0R_G[(\xi+t/2)H_a+\lambda^2J_s(H_a,H_m)]. \quad \text{(A15)}$$

According to Eq. (A14), the critical Josephson current density $J_c^{\rm Jos}$ peaks at a field H_p for which

$$\Phi(H_p,H_m)=0. \quad \text{(A16)}$$

Because $\lambda\gg\xi+t/2$, one can obtain H_p also from $J_s(H_p,H_m)=0$.

[1] L. N. Bulaevskii, L. L. Daemen, M. P. Maley, and J. Y. Coulter, Phys. Rev. B **48**, 13 798 (1993).

[2] K.-H. Müller, C. Andrikidis, H. K. Liu, and S. X. Dou, Phys. Rev. B **50**, 10 218 (1994).

[3] J. R. Clem, Physica C **153–155**, 50 (1988).

[4] J. E. Evetts and B. A. Glowacki, Cryogenics **28**, 641 (1988).

[5] M. E. McHenry, M. P. Maley, and J. O. Willis, Phys. Rev. B **40**, 2666 (1989).

[6] A. A. Zhukov, D. A. Komarkov, G. Karapetrov, S. N. Gordeev, and R. I. Antonov, Supercond. Sci. Technol. **5**, 338 (1992).

[7] K.-H. Müller and D. N. Matthews, Physica C **206**, 275 (1993).

[8] E. Altshuler, J. Musa, J. Barroso, A. R. R. Papa, and V. Venegas, Cryogenics **33**, 308 (1993).

[9] A. I. D'yachenko, Physica C **213**, 167 (1993).

[10] K. Sato, T. Hikata, H. Mukai, M. Ueyama, N. Shibuta, T. Kato, T. Masuda, M. Nagata, K. Iwata, and T. Mitsui, IEEE Trans. Magn. **MAG-27**, 1231 (1991).

[11] R. L. Peterson and J. W. Ekin, Phys. Rev. B **37**, 9848 (1988).

[12] K. Kwasnitza and St. Clerc, Adv. Cryog. Eng. **40**, 53 (1994).
[13] K.-H. Müller, C. Andrikidis, H. K. Liu, and S. X. Dou, Physica C **235–240**, 3037 (1994).
[14] M. R. Cimberle, C. Ferdeghini, R. Flükiger, E. Giannini, G. Grasso, D. Marrè, M. Putti, and A. S. Siri, Physica C **251**, 61 (1995).
[15] H. K. Liu, Y. C. Guo, and S. X. Dou, Supercond. Sci. Technol. **5**, 591 (1992).
[16] J. R. Clem, Phys. Rev. B **43**, 7837 (1991).
[17] A. Majhofer, T. Wolf, and W. Dieterich, Phys. Rev. B **44**, 9634 (1991).
[18] T. Wolf and A. Majhofer, Phys. Rev. B **47**, 5383 (1993).
[19] M. Tinkham and C. J. Lobb, in *Solid State Physics: Advances in Research and Applications*, edited by H. Ehrenreich and D. Turnbull (Academic, New York, 1989), Vol. 42, p. 91.
[20] E. H. Brandt and M. Indenbom, Phys. Rev. B **48**, 12 893 (1993).
[21] F. Zeldov, J. R. Clem, M. McElfresh, and M. Darwin, Phys. Rev. B **49**, 9802 (1994).
[22] E. C. Stoner, Philos. Mag. **36**, 803 (1945).
[23] G. Waysand, Europhys. Lett. **5**, 73 (1988).
[24] M. L. Hodgdon, R. Navarro, and L. J. Campbell, Europhys. Lett. **16**, 677 (1991).
[25] A. Barone and G. Paterno, *Physics and Applications of the Josephson Effect* (Wiley, New York, 1982).
[26] C. P. Bean, Phys. Rev. Lett. **8**, 250 (1962).
[27] C. P. Bean, Rev. Mod. Phys. **36**, 31 (1964).
[28] J. R. Clem and Z. Hao, Phys. Rev. B **48**, 13 774 (1993).
[29] J. R. Cooper, L. Forró, and B. Keszei, Nature (London) **343**, 444 (1990).
[30] A. Schilling, F. Hulliger, and H. R. Ott, Z. Phys. B **82**, 9 (1991).
[31] A. V. Nikulov and D. Yu. Remisov, Supercond. Sci. Technol. **4**, 312 (1991).
[32] L. N. Bulaevskii, J. R. Clem, L. I. Glazman, and A. P. Malozemoff, Phys. Rev. B **45**, 2545 (1992).